npj | materials sustainability

Perspective

https://doi.org/10.1038/s44296-024-00020-0

Sustainable co-production of porous graphitic carbon and synthesis gas from biomass resources

Vishnu Pusarapu[1], Rakesh Narayana Sarma[2], Prince Ochonma[1] & Greeshma Gadikota[1,2] ✉

Existing pathways to produce graphite which include extraction of natural graphite impact the environment, while the conversion of fossil-driven carbon to graphite around temperatures as high as 3000 °C consumes large quantities of energy. Potassium - catalyzed graphitization is a more sustainable route and can achieve graphitic carbon formation at temperatures lower than 1000 °C, while enhancing pore formation and creating porous graphitic carbon (PGC). This two-step approach involves carbonization followed by graphitization. However, the compositions of the gaseous products have not been reported in prior studies. In this perspective, the chemical transformations underlying Alkaline Thermal Graphitization (ATG) for the co-production of synthesis gas (H_2 and CO) and PGC in a single step, utilizing lignocellulosic biomass, are reported. The presence of graphitic and porous carbon structures in PGC are well suited for supercapacitor applications. This promising approach maximizes resource recovery by upgrading volatile matter to synthesis gas and low value biomass residues to porous graphitic carbon (PGC), thus co-producing sustainable fuels and energy storage materials, while lowering CO_2 emissions compared to existing pathways to produce graphite.

Motivation and background

Graphite is a critical resource for accelerating the clean energy transition with key applications in battery electrodes[1], fuel cells[2], solar panel production[3], blades and electric brushes of wind turbines[3], and nuclear reactors[2] due to its excellent mechanical, thermal and electrical conductivity properties[1]. These properties arise from its crystalline structure in which sp^2-hybridized carbon atoms are assembled into a hexagonal ring structure with $\pi - \pi$ stacking arrangements enabled by weak van der Waals interactions[4]. The delocalized electrons in graphite contribute to enhanced mechanical, thermal and electrical conductivity properties.

However, conventional means of producing graphite remain unsustainable. Natural graphite is mined from the earth but has been reported as a supply risk material due to rapidly increasing demand and limited reserves[1]. As an alternative, synthetic graphite is conventionally produced by the Acheson process[5] using coal tar pitch and petroleum coke[6] as the carbon sources. While graphite purity as high as 99.9% is achieved using this process, the need for temperatures as high as ~3000 °C[5], and uncertainties associated with the generation of volatile constituents and their associated environmental impacts challenge the environmental sustainability of this process. Emissions associated with synthetic graphite production have been reported to be as high as 20 kg of CO_2e per kg of graphite[2]. These challenges motivate advances in the development of energy and resource efficient material conversion pathways that facilitate complete utilization of renewable carbonaceous resources to co-produce Porous Graphitic Carbon (PGC) and synthesis gas (or syngas, which is a mixture of CO and H_2) while lowering the greenhouse gas emissions footprint compared to existing graphite production processes.

In the context of harnessing renewable carbon feedstocks[7,8], several studies have highlighted the potential for producing graphite from biomass[9,10]. Lignocellulosic biomass is ubiquitous and comprises a mixture of carbohydrates (~65–75%) and lignin (~18–35%)[11]. Cellulose and hemicellulose are carbohydrates, consisting of glucose, mannose, galactose, xylose, arabinose, 4-O-methylglucoronic acid and galacturonic acid[11]. Lignin is a crosslinked polymer of phenolic compounds mainly comprising three precursors: p-cou-maryl alcohol (I), coniferyl alcohol (II), and sinapyl alcohol (III)[11]. The abundance of lignocellulosic biomass in construction and demolition waste-derived wood and agricultural residues (e.g., coconut shells, rice husks, and sugarcane bagasse) motivates their use for sustainable material and energy conversions[12,13].

[1]Smith School of Chemical and Biomolecular Engineering, Cornell University, Ithaca, NY 14853, USA. [2]School of Civil and Environmental Engineering, Cornell University, Ithaca, NY 14853, USA. ✉e-mail: gg464@cornell.edu

Biomass is conventionally considered to be a challenging feedstock for graphitization due to the formation of turbostratic non-graphitic carbon at temperatures as high as 3000 °C as opposed to graphite formation[14]. In contrast, 'graphitizable' carbons such as petroleum coke form a viscous intermediate at high temperatures and re-arrange to form graphite[15]. It has been hypothesized that the carbonization stage (around 300–500 °C) plays a key role in determining the graphitizability of a carbon precursor. Graphitizable carbons form a 'state of fusion', whereby a viscous carbon phase enables the re-arrangement of carbon to thermodynamically stable graphite planes. In contrast, non-graphitizable carbon precursors undergo cross-linking reactions which impede fusion state formation and carbon re-arrangement[16]. These challenges motivate advances in alternative synthesis pathways to convert biomass to Porous Graphitic Carbon (PGC). Table 1 presents an overview of key parameters in various graphitization processes. As noted in Table 1, the use of potassium – based additives (e.g., KOH, K_2CO_3) lowers the temperatures needed for graphitization.

Catalytic graphitization of biomass

The transformation of carbon precursors into graphite in the presence of a metal catalyst is termed catalytic graphitization. As shown in Fig. 1, two-step or single-step approaches can be harnessed for graphitization. A two-step process typically starts with carbonization or pyrolysis to produce an amorphous carbon-rich porous intermediate. Coconut shells are an excellent source for this purpose as they form char[15] with high carbon content when carbonized. For example, coconut shell char with carbon content greater than 90 wt.% has been reported under slow pyrolysis conditions[13]. As shown in Table 2, palm shell, sugarcane bagasse, cotton stalk, and coconut fiber may also be suitable, given their high biochar content.[13,17]. Process conditions such as the reaction temperature[18] and heating rate[19] influence the composition and yield of biochar. Lignin, a component of lignocellulosic biomass contains an abundance of aromatic groups, and biomass types with high lignin content tend to produce higher char yields and carbon content[20]. Carbon-rich biochar contains aromatic carbon rings[21] which are fused and rearranged to form graphitic layers through catalytic graphitization processes[22]. Alternatively, biomass can be directly mixed with the catalyst and thermochemically treated in a single step to produce graphite[23].

There have been developments in catalytic approaches which involve the use of metal catalysts to generate a molten liquid phase at relatively low temperatures[24], thus promoting the re-arrangement and formation of graphitic structures in a single step using biomass-derived carbon. Iron-based catalysts have been found to form Fe_3C nanoparticles, which melt and dissolve amorphous carbon, and create carbon nanotube structures[23]. Catalytic graphitization of saw dust mixed with Fe or Ni catalysts have been reported at a temperature of 1000 °C resulting in nanosized graphitic structures of high crystallinity. Transition metal nanoparticles promote graphitization at temperatures below 1000 °C[14], forming a variety of 'nanotube', 'nanoribbon', or 'nano-onion' structures, in which graphitic layers are formed locally around the nanoparticle surface, be it stationary or mobile[25]. However, the use of metals such as Fe or Ni is still hindered by the need for acid washing (typically in 1 M HCl[23]) to recover the Fe particles. Excessive use of acid challenges the overall environmental and economic sustainability of graphite production.

Potassium-based catalysts (such as KOH[26], K_2CO_3[27], and K_2FeO_4[28]) are also being explored for their capabilities to simultaneously induce chemical activation and graphitization of biomass-derived carbon at temperatures below 1000 °C without excessive acid requirements for separating catalysts from the product. The mechanism for KOH-mediated activation is outlined through a series of Reactions 1–5 below[28], resulting in the release of organically bound carbon and creation of porosity. KOH reacts with solid carbon resulting in the formation of K_2CO_3 at 400–600 °C[28]. At temperatures greater than 700 °C, K_2CO_3 decomposes to K_2O releasing CO_2 which further activates the carbon, releasing CO and metallic potassium[29]. The Boudouard reaction favors CO production above 680 °C[30]. Potassium-containing compounds have additional catalytic effects on the pyrolytic decomposition of biomass, promoting dehydration, demethoxylation, decarboxylation, decarbonylation, heterocyclic ring opening and catalytic cracking reactions[31]. These pathways suggest that carbohydrates are primarily decomposed to light oxygenates through ring scission reactions, while lignin forms phenolic compounds. Light oxygenates can undergo secondary cracking to gaseous species or contribute to recombination and char formation with lignin-derived compounds.

$$6KOH + 2C \rightarrow 2K + 3H_2 + 2K_2CO_3\,[400 - 600℃] \quad (1)$$

$$K_2CO_3 \rightarrow K_2O + CO_2\,[400 - 600℃] \quad (2)$$

$$CO_2 + C \leftrightarrow 2CO\,[>680℃] \quad (3)$$

Table 1 | Comparison of various chemical pathways for producing graphite and the corresponding experimental conditions

Process (Catalyst)	Carbon source	Synthesis temperature	I_D/I_G[a]	Reaction time	Ref.
Natural	Graphitic ore	–	0.04	–	Kim et al.[73]
Conventional	Petroleum Coke/Coal Tar Pitch	3000 °C	0.069	–	Bogachuk et al.[74]
Electrochemical	Activated Coconut Charcoal	850 °C	0.20	3 h	Thapaliya et al.[35]
Catalytic (Fe)	Pine sawdust	1000 °C	0.381	3 h	Sevilla et al.[14]
Catalytic (Ni)	Pine sawdust	1000 °C	0.661	3 h	Sevilla et al.[14]
Catalytic (K_2CO_3)	Enzymatic Hydrolysis Lignin	900 °C	0.70	2 h	Xi et al.[47]
Catalytic (KOH)	Enzymatic Hydrolysis Lignin	900 °C	0.84	2 h	Xi et al.[47]
Catalytic (K_2CO_3)	Coconut Shell	900 °C	0.088	2 h	Xia et al.[27]
Catalytic (K_2FeO_4)	Bamboo	800 °C	0.86	2 h	Gong et al.[28]
Catalytic ($K_3[Fe(C_2O_4)_3]$)	Eggplant	900 °C	0.74	1 h	Zha et al.[67]
Catalytic (KOH)	Taro starch	700 °C	0.90	2 h	Xing et al.[26]
Microwave Catalytic (Ni)	Activated Carbon	1400 °C	0.304	5 minutes	Kim et al.[75]
Microwave Catalytic (KOH)	Black sesame	700 °C	0.99	20 minutes	Li et al.[37]
Alkaline Thermal Graphitization (KOH)	Wood waste	900 °C	1.75	2 h	Present Work
Two Step Graphitization (KOH)	Wood waste	900 °C	1.70	2 h	Present Work

[a]I_D/I_G is the ratio of 'D' and 'G' peak intensities measured by Raman spectroscopy. A low I_D/I_G is characteristic of pure graphite.

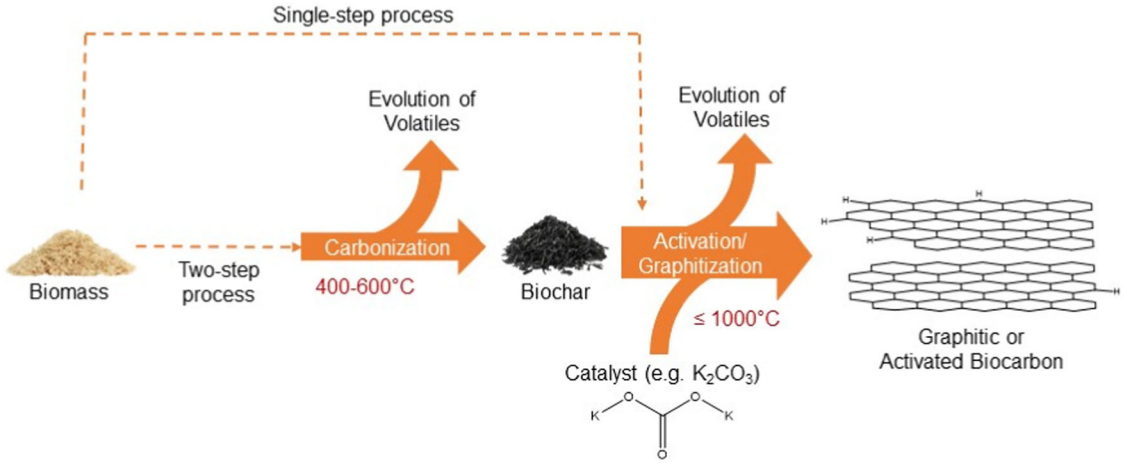

Fig. 1 | Schematic representation of the biomass catalytic graphitization route. In comparison with the single-step process, the two-step process includes an intermediate carbonization step at ~ 400–600 °C to produce carbon-rich biochar prior to activation or graphitization. In a two-step process, biomass first undergoes carbonization to produce a carbon-rich biochar, which is further heated in the presence of a catalyst. A single-step process involves directly mixing the biomass with a catalyst and heating to the desired reaction temperature.

Table 2 | Process conditions and carbon content of synthesized biochar obtained from various biomass sources[13,17]

Biochar type	Synthesis temperature (°C)	Ramp rate (°C/min)	Reaction time	Carbon content (wt%)	Reference
Peanut hull	400	10	1 h	64.00	Kastner et al.[76]
Corncobs	550	15	2 h	81.97	Luo et al.[77]
Sugarcane bagasse	450	10	5 h	88.6	Chin et al.[78]
Palm shell	600	5	1 h	90.6	Windeatt et al.[13]
Pine needle	700	7	3 h	93.70	Ahmad et al.[18]
Woody biomass	550	10	3 h	75.99	Chowdhury et al.[79]
Coconut shell	600	5	1 h	93.9	Windeatt et al.[13]

$$K_2CO_3 + 2C \rightarrow 2K + 3CO\,[>700℃] \quad (4)$$

$$K_2O + C \rightarrow 2K + CO\,[>700℃] \quad (5)$$

The remaining biochar primarily consists of carbon, in the form of sp^2 graphite microcrystals connected by sp^3 hybridized carbons[32]. K_2CO_3 promotes the formation of graphitic structures by two main pathways[27]. The first pathway is a preferential reaction with sp^3 hybridized carbons over sp^2 hybridized carbons during its activation mechanism, removing the cross-links which were previously separating graphite microcrystals. Furthermore, as the temperature reaches around 900 °C and exceeds the melting point of K_2CO_3 (891 °C), the molten salt promotes re-arrangement and combination of graphite microcrystals through the formation of charge transfer complexes and enables the crystallization of amorphous carbon. We have noted the multiple benefits of alkali metal-catalyzed graphitization of biomass including enhanced decomposition and volatilization, catalytic cracking to produce higher gas yields, combined with its beneficial impacts on the quality of char produced such as the creation of micropores and the formation of graphitic structures. However, gas selectivity and the need for separate carbonization and graphitization stages can be improved. The formation of tar in a single-step scheme has been reported to reduce the graphitizing ability of KOH leading to the formation of activated carbon rather than PGC[33] compared to a two-step process, where the volatile tars are released in the carbonization stage prior to graphitization[27]. Moreover, the resulting volatile products of catalytic graphitization processes are generally not studied. There remains scope to tune the composition of the gaseous products for maximum utilization of the biomass resource.

Electrochemical graphitization

Amorphous carbon can also be graphitized by cathodic polarization in a molten $CaCl_2$ electrolyte. High-quality graphitic carbon product has been reported at temperatures of 850 °C[34]. One advantage of the electrochemical method is the absence of a catalyst separation step compared with catalytic graphitization. This approach involves electro-deoxygenation from the surface of carbon precursors which is followed by long-range rearrangement of carbon atoms to transform an amorphous structure to a highly directional nanoflake architecture[34]. Like catalytic graphitization, the electrochemical method has been applied to carbon precursors such as carbon black[34] and coconut char[35]. Significant knowledge gaps remain in our understanding of the underlying reactions, detailed mechanisms, electrolyte stability, the influence of various carbon precursors, and the presence of impurities on electrochemical graphitization[36].

Microwave-induced graphitization

Microwave radiation can potentially increase the degree of graphitization and required reaction times compared to conventional heating methods[37]. In a conventional furnace, heat travels inwards from the surface of the material through heat conduction. In this way, a thermal gradient is formed between the material surface and internal particles, which results in uneven heating of the material contributing to incomplete pore formation and a low specific surface area[37]. In contrast, microwave heating provides rapid heat transfer resulting in complete biomass conversion in 15 minutes[37]. Rapid fluctuations around the temperature set point are hypothesized to promote an improved degree of graphitization by the precipitation-dissolution mechanism[37].

Co-production of porous graphitic carbon and syngas with inherent CO_2 suppression

As an alternative to single step graphitization using alkaline catalysts, Alkaline Thermal Graphitization (ATG) that utilizes both alkaline catalyst as well as a metal catalyst such as nickel to promote gas phase reforming reactions can be tuned to produce highly porous graphitic carbon (PGC), and high purity synthesis gas (H_2 and CO) from lignocellulosic biomass in a single step. ATG is analogous to Alkaline Thermal Treatment (ATT)[38–40], where biomass mixed with alkaline hydroxide results in the production of high purity H_2 by promoting gas phase reforming reactions using a Ni/ZrO_2 (10 wt.%) catalyst at 500 °C[41]. In the proposed ATG process, the Ni/ZrO_2 catalyst alleviates the issue of tar-mediated potassium volatilization[42] in a single-step reaction by promoting catalytic tar cracking reactions. After thermochemical treatment, the produced PGC is washed in a relatively dilute 0.1 M HCl to remove potassium and other impurities. Table 3 shows the gas yields generated by various catalytic thermochemical treatment processes. Factors including the biomass type, reaction temperature and choice of catalyst influence the quantities of gas generated[43]. Evidently, the use of Ni-based catalysts enhances gas production due to catalytic tar cracking. Figure 2 shows the mechanisms associated with ATG. The underlying reactions are summarized in Fig. 3. The overall reaction is as follows:

$$C_xH_yO_z(s) \xrightarrow[Ni/ZrO_2]{KOH} H_2(g) + CO(g) + K_2CO_3(s) + C(s) \quad (6)$$

Materials and methods

To demonstrate the feasibility of ATG, wood material from construction and demolition waste obtained from a processing facility in Cortland, NY, USA was used as a lignocellulosic biomass precursor. Wood was pre-processed by milling, passing through a 1 mm sieve, and drying at 105 °C for 24 h. The composition of the wood is shown in Supplementary Table 1. 1.5 g of wood was then mixed with KOH at a 1:1 mass ratio, and 15 mL water was added to make a slurry, followed by drying at 105 °C for 4 h. Reactants were loaded in a zirconia ceramic crucible and covered by a zirconia ceramic foam filter (VUKOPOR® HT). This mixture was reacted in the presence of 250 mg Ni/ZrO_2 catalyst (10 wt.%) in a separate crucible. The Ni/ZrO_2 catalyst was prepared by a wet impregnation method[41]. The crucibles were loaded into a horizontal tubular furnace, purged with N_2 gas, and heated at a ramp rate of 4 °C/min up to 600 °C and 2 °C/min thereafter until reaching 900 °C and held for 2 h. A constant N_2 flow of 50 cm^3/min was maintained, and the outlet gas flowrate and composition were measured by a mass flowmeter followed by a micro-GC analyzer (Inficon Micro GC Fusion®). The solid product, porous graphitic carbon (PGC) was washed in deionized water and 0.1 M HCl (2 h stirring in each) and dried at 105 °C for 12 h. For comparison, 1.5 g of dried wood was pyrolyzed under a constant N_2 flow to 900 °C under the same furnace settings. Two-step graphitization was performed by carbonizing 1.5 g of dried wood at 400 °C for 3 h (ramp rate of 4 °C/min). The resulting biochar was loaded with KOH in a 1:2 mass ratio as before and heated under a constant N_2 flow to 900 °C under the same furnace settings. PGC was analyzed by Raman Spectroscopy (WITec Alpha 300 R, 785 nm), Scanning/Transmission Electron Microscopy (S/TEM) imaging (Thermo Fisher Spectra 300) and X-ray Photoelectron Spectroscopy (XPS) (Thermo Fisher Nexsa G2). Potassium recovery was measured by ICP-AES (Thermo Fisher ICAP Pro). All experiments were carried out in duplicate.

Results

Based on the generated gas yields shown in Fig. 4a, it is evident that H_2, CO and CO_2 are the main components in the gaseous phase. Alkaline Thermal Graphitization (ATG) yields 21.1 mmol H_2/g biomass, corresponding to a conversion of 55% (relative to the combined H content of biomass and KOH). Significant CO_2 and CO gas yields are due to the decomposition of K_2CO_3 as per its activation mechanism (Reactions 2–5). A yield of 23.5 mmol CO/g biomass was obtained. The H_2/CO ratio is 0.90. As seen in Fig. 4a, there is elevated H_2, CO and CO_2 production (2.1, 2.4 and 1.3 times respectively) compared to pyrolysis of biomass at 900 °C, indicating the enhanced activation of biomass and decomposition of volatiles in the presence of KOH and Ni/ZrO_2 catalyst. Evidently, there is an increase in H_2 and CO evolution with ATG compared to a 'more typical' two-step graphitization with KOH and biomass only. It is primarily a result of the catalytic tar cracking reactions promoted by the Ni/ZrO_2 catalyst in ATG. According to Fig. 4b, the Raman spectrum of the produced PGC shows prominent 'D' and 'G' peaks located at 1340 cm^{-1} and 1584 cm^{-1}, respectively. The 'G' peak corresponds to sp^2 hybridized carbon in an ideal graphitic lattice, whereas the 'D' peak is due to defects in graphitic lattices and the presence of sp^3 hybridized amorphous carbon[44]. The apparent broadening and overlap of these peaks are explained by the presence of two additional peaks, termed 'D3' and 'D4' peaks at 1477 cm^{-1} and 1200 cm^{-1} respectively, corresponding to amorphous carbon and graphitic defects[45]. By fitting these four peaks, the integrated intensity ratio, I_D/I_G, was estimated to be 1.75. Similarly, an I_D/I_G ratio of 1.70 was estimated for the PGC product of two-step graphitization.

Table 1 provides a comparison of the obtained I_D/I_G ratio to those reported in prior publications. Previously, K_2CO_3 activation using coconut shell biomass produced PGC with I_D/I_G ratio as low as 0.088[27], and 0.84 using KOH activation of enzymatic hydrolysis lignin[46]. Here, the higher I_D/I_G ratio indicates a relatively lower graphitic content and higher amorphous C content, primarily due to the difference in the choice of biomass type and activating agent. As shown in Table 2, coconut shells can produce higher graphitic content than wood because they carbonize to form a char with a higher carbon content (and likely greater aromaticity), whereas the presence of heteroatoms in wood char may impede the graphitization process.

Table 3 | Non-condensable gas yield (mmol/g biomass) of various catalytic thermochemical treatment processes using different biomass feedstocks

Carbon source (process)	Catalyst or co-reactants	Synthesis temperature	H_2	CO	CO_2	CH_4	Reference
Corncobs	Limonite	750 °C	21.7	12.5	2.9	3.7	Zhao et al.[80]
Corncobs	Ni/Al_2O_3	750 °C	25.4	13.5	5.2	2.8	Zhao et al.[80]
Pine wood	K_2CO_3	700 °C	4.0	2.6	3.6	0.6	Fan et al.[81]
Seaweed (ATT)	Ni/ZrO_2, Steam, NaOH	500 °C	69.69	0.2	0.2	2.5	Zhang et al.[41]
Pine wood	Ni/Iron Slag	900 °C	23.2	27.3	0.6	4.2	Liu et al.[82]
Pine wood	Ni/Al_2O_3	900 °C	24.9	30.6	0.5	1.2	Liu et al.[82]
Wood waste	–	900 °C	9.9	9.8	5.3	1.4	Present work
Wood waste (2-step graphitization)	KOH	400 °C + 900 °C	7.5	11.5	4.8	0.4	Present work
Wood waste (ATG)	KOH, Ni/ZrO_2	900 °C	21.1	23.5	6.8	0.7	Present work

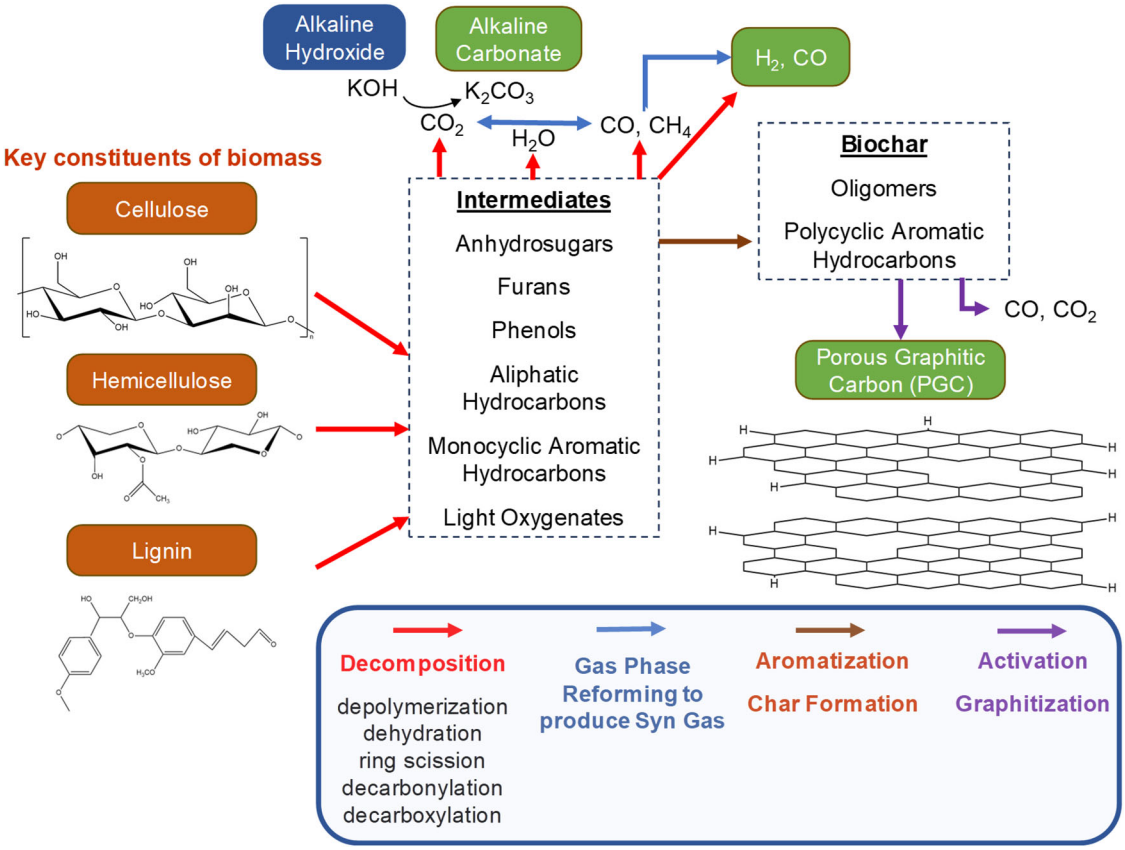

Fig. 2 | Schematic representation of the mechanisms involved in the Alkaline Thermal Graphitization (ATG) process.

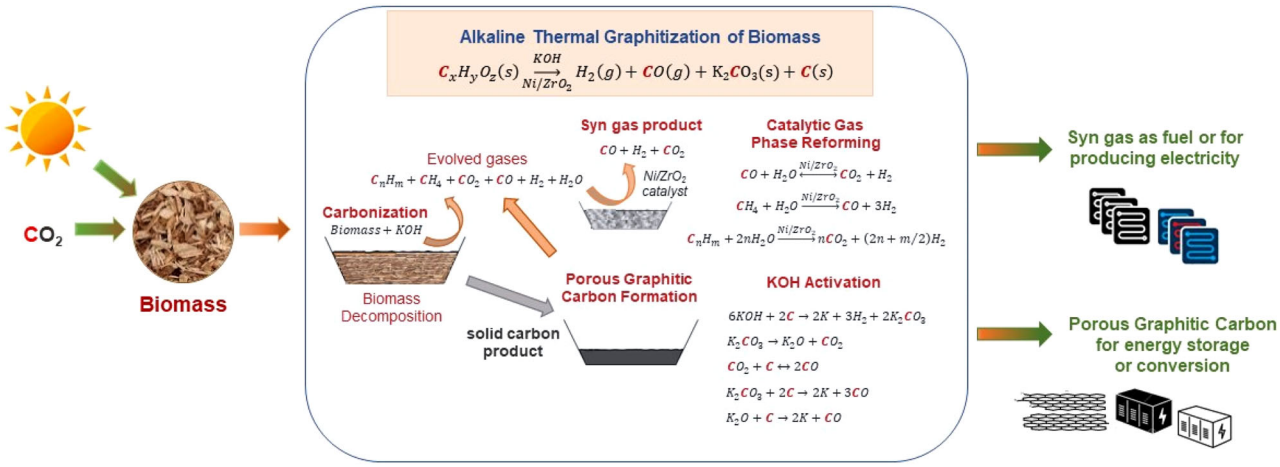

Fig. 3 | Schematic representation of the integrated, single-step alkaline thermal graphitization (ATG) approach to co-produce porous graphitic carbon and syn gas from woody biomass.

Significant oxygen content was detected by XPS analysis (Supplementary Fig. 1). The use of KOH as an activating agent has been thought to reduce the graphitic quality compared to direct use of K_2CO_3, due to greater activation and porosity development, leading to formation of more defects[46]. The I_D/I_G ratios of 1.75 and 1.70 (for ATG and two-step graphitization respectively) are significantly higher than some others in literature[28,37] due to the choice of calculation method. Here, I_D/I_G is reported as a ratio of integrated peak intensities whereas it is often reported as a ratio of peak intensities. If we were to consider the peak intensity ratio, the PGC product of ATG and two-step graphitization would have an I_D/I_G of 1.06 and 0.86 respectively. However, the ratio of integrated intensities is more representative of samples with high defect densities[47]. Figure 4c is a TEM image of a porous graphitic carbon particle. The presence of graphitic planes is evident and the interplanar spacing is found to be 0.50 nm. This observed spacing is larger than the ideal graphite interplanar spacing of 0.335 nm[48], likely due to the intercalation of potassium species[49]. Significant scientific opportunities exist to tune the compositions of PGC to increase the content of graphite, as discussed later.

Sustainability analysis

Alkaline Thermal Graphitization aims to be an environmentally sustainable process for co-producing porous graphitic carbon (PGC) and syngas; thus, an outlook is presented on its potential environmental impacts. A major concern of any thermochemical treatment process is the global warming impact, primarily due to energy consumption of maintaining the high

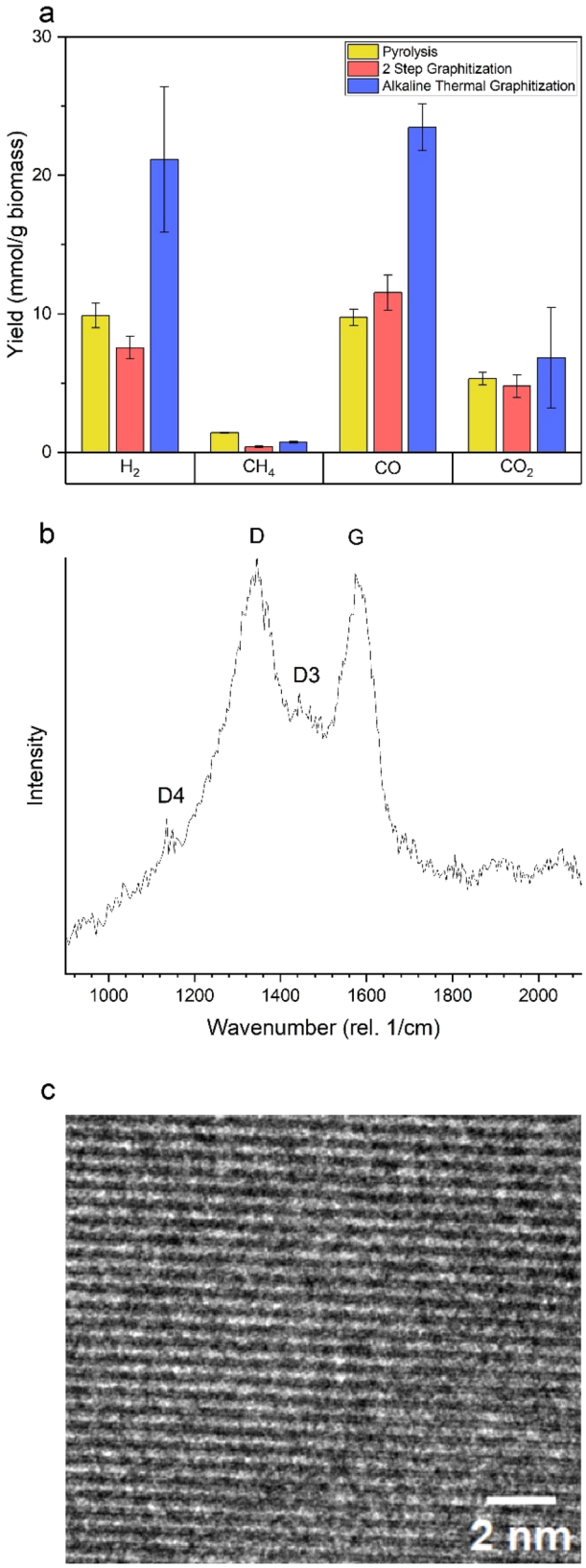

Fig. 4 | Evidence of the formation of porous graphitic carbon (PGC) and syn gas from Alkaline Thermal Graphitization (ATG) of construction and demolition waste wood at 900 °C. a gas yields, **b** evidence of PGC from Raman spectra, and **c** TEM image of PGC.

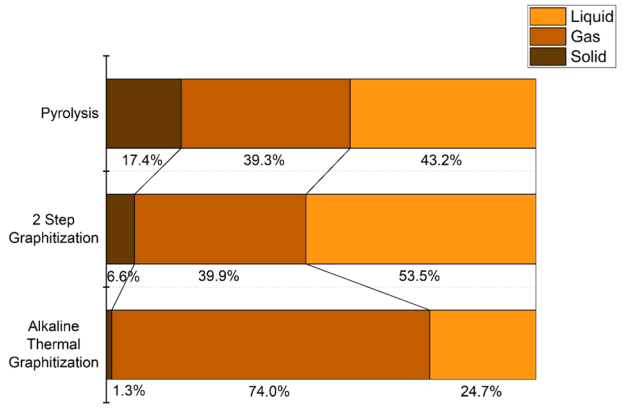

Fig. 5 | Carbon conversion (wt.%) to solid, liquid and gas phase resulting from pyrolysis, two-step graphitization and Alkaline Thermal Graphitization of construction and demolition waste wood at 900 °C.

reaction temperatures required[50]. ATG is preferable in this regard due to the relatively low reaction temperature of 900 °C, as compared to the Acheson process at ~3000 °C[5]. To put this in quantitative context, this is approximately equivalent to an emissions reduction of 840 kg CO_2 per metric ton of carbon produced (based on the heating requirement of graphite[51,52]). CO_2 emissions associated with heating to the required reaction temperature during ATG can be further reduced via integration with solar thermal energy. Direct or indirectly heated solar concentrator systems can be used to heat chemical reactors up to 1100 °C[53]. As biomass acts as a store for atmospheric carbon, combining thermochemical treatment with reduced CO_2 emissions of solar thermal heating can potentially lead to a carbon-negative process. For example, a recent Lifecycle Assessment (LCA) study predicted a solar thermal biomass gasification process to have net negative global warming potential impact[54]. Another consideration is material utilization efficiency. Figure 5 shows the carbon balance of the processes, comparing the carbon conversion of ATG with two-step graphitization and pyrolysis processes. Carbon content in the solid phase was calculated using XPS measurements (Supplementary Figure 1, Supplementary Table 2). ATG has the highest rate of carbon utilization, with a combined solid and gas conversion of 75.3%, compared to 46.5% for two-step graphitization and 56.8% for pyrolysis. Figure 5 also shows that the conversion of carbon to the solid phase decreases from 17.4% for pyrolysis to 1.3% for ATG. It is believed that the presence of KOH in ATG promotes volatilization of carbon (reactions 1–5) and as a result, more carbon is converted to the gas phase. The solid carbon yield of two-step graphitization is intermediate, at 6.6% as KOH is added after the char formation step. ATG leads to lower solid carbon yields as Ni/ZrO_2-promoted catalytic tar cracking of volatiles is favored over recombination and secondary char forming reactions[21].

KOH utilization is also another major consideration for the environmental sustainability of ATG. Washing in 30% HCl has been predicted to recover potassium and thus can bring down the ecotoxicity impacts by up to 60% compared to activation without the recovery step[55]. By lowering the acid consumption required with ATG, we can further reduce the associated ecotoxicity impacts. Potassium-catalyzed graphitization results in formation of metallic K (reaction 5). This can intercalate into the graphite and can be converted back to KOH by washing, accompanied by evolution of H_2 as per the following reaction[56]:

$$C_8K + H_2O \rightarrow 8C(graphite) + KOH + \frac{1}{2}H_2 \quad (7)$$

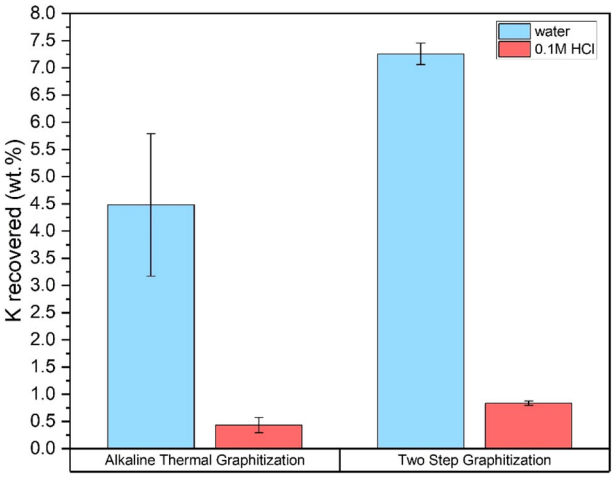

Fig. 6 | Potassium recovered from deionized water and 0.1 M HCl washing steps in Alkaline Thermal Graphitization and two-step graphitization.

There is potential to harness the additional H_2 generated during the recovery of KOH. However, reaction with water alone does not remove all potassium from the solid phase[57]. 2 M HCl has been used in prior works[26,37] for potassium removal. In this study, PGC was washed in a more dilute 0.1 M HCl after an initial water wash with 2 h of stirring in each step. The amount of potassium recovered during washing, relative to the initial KOH loading, is shown in Fig. 6. Potassium recovered by two-step graphitization (8.1%) is higher than that of ATG (4.9%), corresponding to the greater solid carbon yield, in which slightly more potassium was trapped. In both cases, the volatilization of potassium above 800 °C[58] is limiting potassium recovery, with potassium being released in the vapor phase. Condensed vapors remaining on the walls of the tubular furnace after ATG were analyzed by XPS (Supplementary Figure 1) and show elevated potassium levels. Volatilization of potassium is also a practical issue, leading to reactor corrosion. Minor amounts of potassium may remain in the PGC product after washing, as seen in the XPS spectrum of ATG char (Supplementary Fig. 1), although it was only observed in a single sample. The concentration of HCl and time required for complete potassium removal requires further optimization. While the sustainability analysis has been done by assuming the final application of the PGC is in replacing graphite in battery electrodes, it is important to note that there remains scope for further process optimization of ATG to achieve a higher degree of graphitization for several other applications. Improving PGC yields will be crucial to maximize the economic viability of ATG since the current value of graphite (>$70,000 per metric ton[2]) is higher than that of syngas (~$700 per metric ton[59]).

Key conclusions, research directions, and opportunities

The Alkaline Thermal Graphitization (ATG) of low value biomass residues has promising potential for sustainable, carbon-negative production of porous graphitic carbon (PGC), a versatile material for energy storage and conversion. The combination of porous and graphitic structures in PGC make it well suited for supercapacitor applications[22]. Amorphous carbon with a porous structure contributes to elevated electrochemical active surface area and improves the overall capacity. Hence, biomass-derived activated carbon is an effective supercapacitor material[60]. A hierarchical porous structure facilitates rapid ion transport[61] due to micropores contributing to a large surface area, while mesopores provide ion transport channels and macropores act as electrolyte reservoirs. Graphitic carbon further improves performance by enhancing electrical conductivity[24]. PGC generated by ATG has comparable graphitic quality to prior studies which used similar carbon materials as electrodes in lithium-ion batteries[46] and supercapacitors[28] and found significant performance improvements. Gong et al. [28] produced PGCs with I_D/I_G ratio 0.86 from bamboo and obtained energy densities ranging from 3.3 to 16.7 W h kg^{-1}, compared to 4 to 5 W h kg^{-1} of commercial activated carbon-based supercapacitors. Similarly, Xi et al. [46] produced lignin-derived PGC has an I_D/I_G ratio of 0.70 and maintained a specific capacity of 520 mA h g^{-1}, higher than other carbon-based electrodes. Thus, it is predicted that ATG-derived PGC will show promise as an electrode material for supercapacitors or lithium-ion batteries. ATG offers several transformative benefits over conventional synthetic graphite. First, ATG reduces the detrimental environmental impacts from conventional graphite production, limits emissions of greenhouse gases and other harmful volatile gases and reduces tar generation. Second, the co-production of PGC and syngas leads to comprehensive utilization of low value and locally available biomass residues and generates additional revenue for farmers. Third, the relatively lower temperature at which ATG occurs, which is 1000 °C or lower compared to 3000 °C required for thermal graphitization, enables ease of integration with renewable solar thermal energy. Fourth, lignin which has limited uses is ideally suited for ATG. Approaches that can effectively separate cellulosic and hemicellulosic biomass components for alternate applications, while directing lignin for ATG can unlock the complete value of heterogeneous biomass resources.

Several key opportunities can be further explored to tune ATG. First, approaches to lower the temperature for ATG need to be developed to improve potassium recovery. The addition of other salts can lower the melting point by eutectic formation and promote graphitization at lower temperatures. For example, it has been found that a mixture of K_2CO_3 and $Ca(OH)_2$ with coal forms a eutectic mixture around 525 °C[62]. Alternatively, Na_2CO_3 and K_2CO_3 can be combined to make a eutectic mixture with a melting point of 710 °C[63]. Second, the role of steam in ATG needs to be resolved. It is hypothesized that the addition of steam can enhance tar cracking reactions in the presence of the Ni/ZrO_2 catalyst and further improve the graphitic quality of the carbon product by reducing the concentration of tar in the system. However, it is also important to note that steam-enhanced cracking reactions could also reduce solid carbon yields further. Another concern is the steam promoted volatilization of K_2CO_3 by conversion to KOH at temperatures of 800 °C or greater[64]. Third, $MgCl_2$ can also be considered as a useful reagent in promoting the conversion of phenols to polycyclic aromatic hydrocarbons (PAHs) and oligomers in the solid product[65], thereby improving char yields and aromaticity. K_2CO_3, Na_2CO_3 and $MgCl_2$ can all be later recovered by water washing. Fourth, tuning the reaction temperature for ATG can have unintended consequences that need to be resolved. For example, CO and CO_2 evolution reactions can potentially be suppressed by limiting the maximum temperature to 700 °C[58]. However, this temperature is not sufficient for molten salt formation and graphitization with K_2CO_3 alone. In theory, if K_2CO_3 remains stable in the solid phase, it can be trivially separated post-reaction by water washing and recovered, either to be stored as a stable carbon sink or otherwise utilized. Fifth, there is potential to explore synthesis routes which produce increased graphitic quality PGC. The combination of transition metal-catalyzed and potassium-catalyzed graphitization has been found to induce more graphitic carbon formation than potassium-based methods alone[28,66]. Such methods involve the use of reagents which contain both iron and potassium, e.g. K_2FeO_4[28] and $K_3[Fe(C_2O_4)_3]$[66], releasing the metals upon decomposition. However, the multi-step synthesis of such salts[67,68] adds complexity and likely increases the environmental footprint of the process. As a more sustainable alternative, there remains scope to harness plant materials with elevated metal content derived from phytomining or agromining of previously mined or low productivity agricultural lands[69]. More than 520 nickel-hyperaccumulating plant species[70] can potentially provide a source of Ni-rich biomass for improved ATG without the need for additional synthetic metal-bearing reagents, while also remediating poor quality or polluted soils. Lastly, opportunities for whole system integration including lignin separation from low value biomass resources, co-production of porous graphitic carbon and syngas, and syngas utilization for electricity generation in a fuel cell[71], or conversion into liquid hydrocarbon fuels by Fischer-Tropsch Synthesis or commodity chemicals such as methanol[72], need to be evaluated in more detail for life cycle and economic impacts. Exploration of these opportunities will enable successful scalable

and transformative advances in the co-production of porous graphitic carbon and syngas from renewable and low value biomass resources with inherent suppression of CO_2 emissions. These pathways are crucial for closing material cycles and creating a resilient supply chain of critical materials for a sustainable future.

Data availability

Data is provided within the manuscript.

Received: 30 December 2023; Accepted: 8 March 2024;
Published online: 02 July 2024

References

1. Robinson, G. G. R., Hammarstrom, J. M. & Olsen, D. W. *Graphite.* U.S. Geological Survey Professional Paper 1802–J. (U.S. Geological Survey, 2017).
2. Zhang, J., Liang, C. & Dunn, J. B. Graphite Flows in the U.S.: Insights into a Key Ingredient of Energy Transition. *Environ. Sci. Technol.* **57**, 3402–3414 (2023).
3. European Carbon and Graphite Association. *Towards CO2 Neutrality Due to Carbon and Graphite* (European Carbon and Graphite Association, 2019).
4. Chung, D. D. L. Review Graphite. *J. Mater. Sci.* **37**, 1475–1489 (2002).
5. Guichelaar, P. J. Acheson Process. In *Carbide, Nitride and Boride Materials Synthesis and Processing* (ed. Weimer, A. W.) 115–129 (Springer Netherlands, Dordrecht, 1997). https://doi.org/10.1007/978-94-009-0071-4_4.
6. Tamashausky, A.V. *An Introduction to Synthetic Graphite.* (Asbury Graphite Mills Inc, 2006).
7. Ochonma, P., Blaudeau, C., Krasnoff, R. & Gadikota, G. Exploring the Thermodynamic Limits of Enhanced H2 Recovery With Inherent Carbon Removal From Low Value Aqueous Biomass Oxygenate Precursors. *Front. Energy Res*. **9**, 742323 (2021).
8. Ochonma, P., Noe, C., Mohammed, S., Mamidala, A. & Gadikota, G. Integrated low carbon H_2 conversion with *in situ* carbon mineralization from aqueous biomass oxygenate precursors by tuning reactive multiphase chemical interactions. *React. Chem. Eng.* **8**, 1943–1959 (2023).
9. Sinha, P., Banerjee, S. & Kar, K. K. Characteristics of Activated Carbon. in *Handbook of Nanocomposite Supercapacitor Materials I* 125–154 (Springer Nature, Cham, Switzerland, 2020). https://doi.org/10.1007/978-3-030-43009-2_4.
10. Banek, N. A., McKenzie, K. R., Abele, D. T. & Wagner, M. J. Sustainable conversion of biomass to rationally designed lithium-ion battery graphite. *Sci. Rep.* **12**, 8080 (2022).
11. Pettersen, R. C. The Chemical Composition of Wood. In *The Chemistry of Solid Wood* (ed. Rowell, R.) vol. 207 57–126 (American Chemical Society, Washington, DC, 1984).
12. Khodaei, H. et al. Multi-objective utilization of wood waste recycled from construction and demolition (C&D): Products and characterization. *Waste Manag.* **149**, 228–238 (2022).
13. Windeatt, J. H. et al. Characteristics of biochars from crop residues: Potential for carbon sequestration and soil amendment. *J. Environ. Manage* **146**, 189–197 (2014).
14. Sevilla, M., Sanchís, C., Valdés-Solís, T., Morallón, E. & Fuertes, A. B. Synthesis of Graphitic Carbon Nanostructures from Sawdust and Their Application as Electrocatalyst Supports. *J. Phys. Chem. C* **111**, 9749–9756 (2007).
15. Kurzweil, P. & Brandt, K. Overview of Rechargeable Lithium Battery Systems. in *Electrochemical Power Sources: Fundamentals, Systems, and Applications* 47–82 (Elsevier, 2019). https://doi.org/10.1016/B978-0-444-63777-2.00003-7.
16. Kipling, J. J., Sherwood, J. N., Shooter, P. V. & Thompson, N. R. Factors influencing the graphitization of polymer carbons. *Carbon N. Y.* **1**, 315–320 (1964).
17. Chen, W.-H. et al. Biomass-derived biochar: From production to application in removing heavy metal-contaminated water. *Process Saf. Environm. Prot.* **160**, 704–733 (2022).
18. Ahmad, M. et al. Trichloroethylene adsorption by pine needle biochars produced at various pyrolysis temperatures. *Bioresour. Technol.* **143**, 615–622 (2013).
19. Angın, D. Effect of pyrolysis temperature and heating rate on biochar obtained from pyrolysis of safflower seed press cake. *Bioresour. Technol.* **128**, 593–597 (2013).
20. Tomczyk, A., Sokołowska, Z. & Boguta, P. Biochar physicochemical properties: pyrolysis temperature and feedstock kind effects. *Rev. Environ. Sci. Biotechnol.* **19**, 191–215 (2020).
21. Collard, F.-X. & Blin, J. A review on pyrolysis of biomass constituents: Mechanisms and composition of the products obtained from the conversion of cellulose, hemicelluloses and lignin. *Renew. Sustain. Energy Rev.* **38**, 594–608 (2014).
22. Zhang, X. et al. Porous and graphitic structure optimization of biomass-based carbon materials from 0D to 3D for supercapacitors: A review. *Chem. Eng. J.* **460**, 141607 (2023).
23. Thompson, E., Danks, A. E., Bourgeois, L. & Schnepp, Z. Iron-catalyzed graphitization of biomass. *Green Chem.* **17**, 551–556 (2015).
24. Chen, Q. et al. Biomass-derived porous graphitic carbon materials for energy and environmental applications. *J. Mater. Chem. A Mater.* **8**, 5773–5811 (2020).
25. Goldie, S. J. & Coleman, K. S. Graphitization by Metal Particles. *ACS Omega* **8**, 3278–3285 (2023).
26. Xing, L. et al. Synthesis of Porous Carbon Material with Suitable Graphitization Strength for High Electrochemical Capacitors. *ACS Sustain. Chem. Eng.* **7**, 6601–6610 (2019).
27. Xia, J. et al. Three-dimensional porous graphene-like sheets synthesized from biocarbon *via* low-temperature graphitization for a supercapacitor. *Green Chem.* **20**, 694–700 (2018).
28. Gong, Y., Li, D., Luo, C., Fu, Q. & Pan, C. Highly porous graphitic biomass carbon as advanced electrode materials for supercapacitors. *Green Chem.* **19**, 4132–4140 (2017).
29. Lozano-Castelló, D., Calo, J. M., Cazorla-Amorós, D. & Linares-Solano, A. Carbon activation with KOH as explored by temperature programmed techniques, and the effects of hydrogen. *Carbon N. Y.* **45**, 2529–2536 (2007).
30. Speight, J. G. Upgrading by Gasification. In *Heavy Oil Recovery and Upgrading* 559–614 (Elsevier, Cambridge, MA, 2019). https://doi.org/10.1016/B978-0-12-813025-4.00013-1.
31. Wang, W., Lemaire, R., Bensakhria, A. & Luart, D. Review on the catalytic effects of alkali and alkaline earth metals (AAEMs) including sodium, potassium, calcium and magnesium on the pyrolysis of lignocellulosic biomass and on the co-pyrolysis of coal with biomass. *J. Anal. Appl. Pyrolysis* **163**, 105479 (2022).
32. Chen, Y., Zhang, X., Chen, W., Yang, H. & Chen, H. The structure evolution of biochar from biomass pyrolysis and its correlation with gas pollutant adsorption performance. *Bioresour. Technol.* **246**, 101–109 (2017).
33. Adinata, D., Wandaud, W. & Aroua, M. Preparation and characterization of activated carbon from palm shell by chemical activation with K2CO3. *Bioresour. Technol.* **98**, 145–149 (2007).
34. Jin, X., He, R. & Dai, S. Electrochemical Graphitization: An Efficient Conversion of Amorphous Carbons to Nanostructured Graphites. *Chem. Europ. J.* **23**, 11455–11459 (2017).
35. Thapaliya, B. P. et al. Low-Cost Transformation of Biomass-Derived Carbon to High-Performing Nano-graphite via Low-Temperature Electrochemical Graphitization. *ACS Appl. Mater Interfaces* **13**, 4393–4401 (2021).
36. Zaikov, Y. P. et al. Calcium Production by the Electrolysis of Molten CaCl2—Part I. Interaction of Calcium and Copper-Calcium Alloy with Electrolyte. *Metall. Mater. Trans. B* **45**, 961–967 (2014).

37. Li, T., Ma, R., Xu, X., Sun, S. & Lin, J. Microwave-induced preparation of porous graphene nanosheets derived from biomass for supercapacitors. *Microporous Mesoporous Mater.* **324**, 111277 (2021).
38. Asgar, H., Mohammed, S., Kuzmenko, I. & Gadikota, G. Relating Structural and Microstructural Evolution to the Reactivity of Cellulose and Lignin during Alkaline Thermal Treatment with Ca(OH) 2 for Sustainable Energy Production Integrated with CO 2 Capture. *ACS Sustain. Chem. Eng.* **7**, 5449–5461 (2019).
39. Ferguson, T. E., Park, Y., Petit, C. & Park, A. H. A. Novel approach to hydrogen production with suppressed CO x generation from a model biomass feedstock. *Energy Fuels* **26**, 4486–4496 (2012).
40. Stonor, M. R., Ferguson, T. E., Chen, J. G. & Park, A. H. A. Biomass conversion to H2 with substantially suppressed CO2 formation in the presence of Group I & Group II hydroxides and a Ni/ZrO2 catalyst. *Energy Environ. Sci.* **8**, 1702–1706 (2015).
41. Zhang, K., Kim, W. J. & Park, A. H. A. Alkaline thermal treatment of seaweed for high-purity hydrogen production with carbon capture and storage potential. *Nat. Commun.* **11**, 3783 (2020).
42. Long, J. et al. Release characteristics of alkali and alkaline earth metallic species during biomass pyrolysis and steam gasification process. *Bioresour. Technol.* **116**, 278–284 (2012).
43. Gao, Y. et al. Syngas Production from Biomass Gasification: Influences of Feedstock Properties, Reactor Type, and Reaction Parameters. *ACS Omega* **8**, 31620–31631 (2023).
44. Pimenta, M. A. et al. Studying disorder in graphite-based systems by Raman spectroscopy. *Phys. Chem. Chem. Phys.* **9**, 1276–1290 (2007).
45. Sadezky, A., Muckenhuber, H., Grothe, H., Niessner, R. & Pöschl, U. Raman microspectroscopy of soot and related carbonaceous materials: Spectral analysis and structural information. *Carbon N. Y.* **43**, 1731–1742 (2005).
46. Xi, Y. et al. K2CO3 activation enhancing the graphitization of porous lignin carbon derived from enzymatic hydrolysis lignin for high performance lithium-ion storage. *J. Alloys Compd.* **785**, 706–714 (2019).
47. Jorio, A. et al. Measuring disorder in graphene with the G and D bands. *Phys. Status Solidi* **247**, 2980–2982 (2010).
48. Serp, P. Carbon. In *Comprehensive Inorganic Chemistry II* 323–369 (Elsevier, 2013). https://doi.org/10.1016/B978-0-08-097774-4.00731-2.
49. Wang, S., Wang, C. & Ji, X. Towards understanding the salt-intercalation exfoliation of graphite into graphene. *RSC Adv.* **7**, 52252–52260 (2017).
50. Li, G. et al. Life cycle energy consumption and GHG emissions of biomass-to-hydrogen process in comparison with coal-to-hydrogen process. *Energy* **191**, 116588 (2020).
51. Butland, A. T. D. & Maddison, R. J. The specific heat of graphite: An evaluation of measurements. *J. Nucl. Mater.* **49**, 45–56 (1973).
52. EPA. *U.S. National Weighted Average CO2 Marginal Emission Rate, Year 2021 Data*. https://www.epa.gov/avert. https://www.epa.gov/avert (2022).
53. Sheu, E. J., Mokheimer, E. M. A. & Ghoniem, A. F. A review of solar methane reforming systems. *Int. J. Hydrogen Energy* **40**, 12929–12955 (2015).
54. Fang, Y. et al. Life cycle assessment and cost benefit analysis of concentrated solar thermal gasification of biomass for continuous electricity generation. *Energy* **284**, 128709 (2023).
55. Adlak, K., Chandra, R., Kumar, V., Pant, K. K. & Vijay, V. K. Life cycle assessment as a comparison tool for activated carbon preparations and biomethane storage for vehicular applications. *Int. J. Energy Res.* **46**, 17362–17375 (2022).
56. Schlögl, R. & Boehm, H. P. The reaction of potassium-graphite intercalation compounds with water. *Carbon N .Y.* **22**, 351–358 (1984).
57. Ebert, L. B., Mills, D. R., Garcia, A. R. & Scanlon, J. C. More on the reaction of graphite/potassium with water. *Mater. Res. Bull.* **20**, 1453–1460 (1985).
58. Jensen, P. A., Frandsen, F. J., Dam-Johansen, K. & Sander, B. Experimental Investigation of the Transformation and Release to Gas Phase of Potassium and Chlorine during Straw Pyrolysis. *Energy Fuels* **14**, 1280–1285 (2000).
59. Rezaei, E. & Dzuryk, S. Techno-economic comparison of reverse water gas shift reaction to steam and dry methane reforming reactions for syngas production. *Chem. Eng. Res. Des.* **144**, 354–369 (2019).
60. Saini, S., Chand, P. & Joshi, A. Biomass derived carbon for supercapacitor applications: Review. *J. Energy Storage* **39**, 102646 (2021).
61. Ding, C. et al. An in-situ Blowing-etching strategy for preparation of Macro-meso-micro hierarchical porous carbon and its supercapacitive property. *Appl. Surf. Sci.* **569**, 151057 (2021).
62. Hu, J., Liu, L., Cui, M. & Wang, J. Calcium-promoted catalytic activity of potassium carbonate for gasification of coal char: The synergistic effect unrelated to mineral matter in coal. *Fuel* **111**, 628–635 (2013).
63. Zhang, G. et al. Study on the influence of glass encapsulating on the hygroscopicity of high temperature phase change heat storage materials. *IOP Conf. Ser. Earth Environ. Sci.* **474**, 052094 (2020).
64. Zhao, H., Xu, W., Song, Q., Zhuo, J. & Yao, Q. Effect of Steam and SiO_2 on the Release and Transformation of K_2CO_3 and KCl during Biomass Thermal Conversion. *Energy Fuels* **32**, 9633–9639 (2018).
65. Hwang, H., Oh, S., Choi, I.-G. & Choi, J. W. Catalytic effects of magnesium on the characteristics of fast pyrolysis products – Bio-oil, bio-char, and non-condensed pyrolytic gas fractions. *J. Anal. Appl. Pyrolysis* **113**, 27–34 (2015).
66. Zha, Z. et al. One-step preparation of eggplant-derived hierarchical porous graphitic biochar as efficient oxygen reduction catalyst in microbial fuel cells. *RSC Adv.* **11**, 1077–1085 (2021).
67. Baran, E. J. Natural iron oxalates and their analogous synthetic counterparts: A review. *Geochemistry* **76**, 449–460 (2016).
68. Okaikue-Woodi, F. E. K. & Ray, J. R. Synthesis of ferrate (Fe(VI))-coated sand for stabilized reactivity and enhanced treatment of phenol. *J. Mater. Chem. A Mater.* **11**, 13552–13563 (2023).
69. van der Ent, A. et al. Agromining: Farming for Metals in the Future? *Environ. Sci. Technol.* **49**, 4773–4780 (2015).
70. Laubie, B., Vaughan, J. & Simonnot, M.-O. Processing of Hyperaccumulator Plants to Nickel Products. In: *Agromining: Farming for Metals* (eds. van der Ent, A., J.M. Baker, A., Echevarria, G., Simonnot, M.-O. & Morel, J. L.) 47–61 (Springer Nature Switzerland AG, Cham, Switzerland, 2021). https://doi.org/10.1007/978-3-030-58904-2_3.
71. da Rosa, A. V. & Ordóñez, J. C. Hydrogen Production. In *Fundamentals of Renewable Energy Processes* 419–470 (Elsevier, 2022). https://doi.org/10.1016/B978-0-12-816036-7.00021-X.
72. Rauch, R., Hrbek, J. & Hofbauer, H. Biomass gasification for synthesis gas production and applications of the syngas. *WIREs Energy Environ.* **3**, 343–362 (2014).
73. Kim, S.-G., Park, O.-K., Lee, J. H. & Ku, B.-C. Layer-by-layer assembled graphene oxide films and barrier properties of thermally reduced graphene oxide membranes. *Carbon Lett.* **14**, 247–250 (2013).
74. Bogachuk, D. et al. Comparison of highly conductive natural and synthetic graphites for electrodes in perovskite solar cells. *Carbon N. Y.* **178**, 10–18 (2021).
75. Kim, T., Lee, J. & Lee, K.-H. Full graphitization of amorphous carbon by microwave heating. *RSC Adv.* **6**, 24667–24674 (2016).
76. Kastner, J. R. et al. Catalytic esterification of fatty acids using solid acid catalysts generated from biochar and activated carbon. *Catal Today* **190**, 122–132 (2012).

77. Luo, M. et al. Efficient simultaneous removal of cadmium and arsenic in aqueous solution by titanium-modified ultrasonic biochar. *Bioresour. Technol.* **284**, 333–339 (2019).
78. Chin, L. H., Abdullah, A. Z. & Hameed, B. H. Sugar cane bagasse as solid catalyst for synthesis of methyl esters from palm fatty acid distillate. *Chem. Eng. J.* **183**, 104–107 (2012).
79. Chowdhury, Z. Z., Karim, Md. Z., Ashraf, M. A. & Khalid, K. Influence of Carbonization Temperature on Physicochemical Properties of Biochar derived from Slow Pyrolysis of Durian Wood (Durio zibethinus) Sawdust. *Bioresources* **11**, 3356–3372 (2016).
80. Zhao, X.-Y. et al. Catalytic Reforming of Volatiles from Biomass Pyrolysis for Hydrogen-Rich Gas Production over Limonite Ore. *Energy Fuels* **31**, 4054–4060 (2017).
81. Fan, H., Chang, X., Wang, J. & Zhang, Z. Catalytic pyrolysis of agricultural and forestry wastes in a fixed-bed reactor using K_2CO_3 as the catalyst. *Waste Manag. Res.* **38**, 78–87 (2020).
82. Ma, T., Liu, Y. & Yu, H. Catalytic characteristics of pyrolysis volatile matter from biomass/biomass components on a novel Ni-based catalyst supported by iron slag. *J. Renew. Sustain. Energy* **9**, 063101 (2017).

Acknowledgements

The authors acknowledge the use of the shared facilities at the Cornell Center for Materials Research (CCMR) which are supported through the National Science Foundation Materials Research Science and Engineering Centers (NSF MRSEC) program (DMR-1719875). V.P. and G.G.'s contributions are supported by the ARPA-E OPEN/MINER Program through DE-AR0001608. P.O.'s efforts are supported by the Link Foundation Energy Fellowship. Special thanks to Akanksh Mamidala and Shree K. Giri for carrying out ICP- AES testing.

Author contributions

V.P. developed the procedure for alkaline thermal graphitization, conducted the experiments, analyzed and plotted the data, contributed to literature review, writing and editing of the manuscript. R.N.S. supported literature review and contributed to writing and editing the manuscript. P.O. conducted the XPS measurements, edited the manuscript and contributed to the analyses of biomass valorization pathways. G.G. proposed the concept of single-step co-production of PGC and syngas from biomass, oversaw the development and execution of the concept and experimental plan, and edited the manuscript. All authors reviewed the manuscript.

Competing interests

The corresponding author, G.G., is an Associate Editor of npj Materials Sustainability. For this reason, she cannot serve as the reviewer or the editor for this manuscript.

Additional information

Supplementary information The online version contains supplementary material available at https://doi.org/10.1038/s44296-024-00020-0.

Correspondence and requests for materials should be addressed to Greeshma Gadikota.